ACS OMEGA

http://pubs.acs.org/journal/acsodf

Article

Development of a Theoretical Model That Predicts Optothermal Energy Conversion of Gold Metallic Nanoparticles

Nahid Rafiei,[¶] Hossein Alishah Aratboni,[¶] Larousse Khosravi Khorashad, Abbas Alemzadeh,* Sadasivan Shaji, and José Rubén Morones Ramírez*

Cite This: *ACS Omega* 2020, 5, 1377−1383

Read Online

ACCESS | Metrics & More | Article Recommendations

ABSTRACT: Gold nanoparticles (AuNPs) can be found in different shapes and sizes, which determine their chemical and physical characteristics. Physical and chemical properties of metallic NPs can be tuned by changing their shape, size, and surface chemistry; therefore, this has led to their use in a wide variety of applications in many industrial and academic sectors. One of the features of metallic NPs is their ability to act as optothermal energy converters, where they absorb light at a specific wavelength and heat up their local nanosurfaces. This feature has been used in many applications where metallic NPs get coupled with thermally responsive systems to trigger an optical response. In this study, we synthesized AuNPs that are spherical in shape with an average diameter of 20.07 nm. This work assessed simultaneously theoretical and experimental techniques to evaluate the different factors that affect heat generation at the surface of AuNPs when exposed to a specific light wavelength. The results indicated that laser power, concentration of AuNPs, time × laser power interaction, and time illumination, were the most important factors that contributed to the temperature change exhibited in the AuNPs solution. We report a regression model that allows predicting heat generation and temperature changes with residual standard errors of less than 4%. These results are highly relevant in the future design and development of applications where metallic NPs are incorporated into systems to induce a temperature change triggered by light exposure.

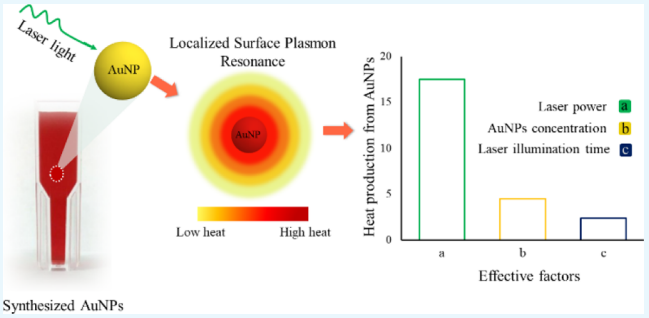

1. INTRODUCTION

Nanotechnology is an interdisciplinary scientific field which involves designing and manipulating atoms and molecules to form extremely small structures.[1] Some examples of these structures are nanoparticles (NPs) which have gained extensive use in different fields such as computer science,[2] electronics,[3,4] chemistry,[5] biotechnology,[6−8] and medicine.[9−14] Gold nanoparticles (AuNPs) are among the most commonly used NPs because of their unique physical and chemical properties, particularly their lack of toxicity to biological systems, which allows them to be compatible to be incorporated into diverse systems in the food industry, cosmetics, optics, and biomaterial production.[15] One of the most utilized properties of AuNPs is their capability of converting optical energy of specific wavelengths into thermal energy.

The ability of metallic NPs to convert absorbed light into heat is due to the surface plasmon resonance exhibited only when the metal is at the nanoscale. The NPs present electron−phonon and phonon−phonon interactions, and part of the high-energy excited plasmon can decay via a nonradiative process, leading to the release of thermal energy. Ultimately, this thermal energy produced causes an increase in the temperature of the surroundings of the nanostructure that diffuses away from the surface of the hot metallic NPs. This effect happening globally in a homogenous NP solution leads to an elevation in the temperature of the bulk solution harboring the NPs.[16−20] This physical property of the nanostructures has led to their applications in cancer imaging,[21] cancer cell ablation,[22] spectroscopic detection,[23] photothermal therapy,[24] and gene silencing.[25]

In each one of these applications, depending on the desired conditions and aims, two forms of laser light [pulsed and continuous wave (CW)] have been used to supply optical energy at a specific wavelength. In spite of heat production required at the mentioned applications, the lack of quantification in the heat generation in most of these applications has led to methodological and experimental difficulties in the operative procedure and additional

Received: August 10, 2019
Accepted: December 31, 2019
Published: January 14, 2020

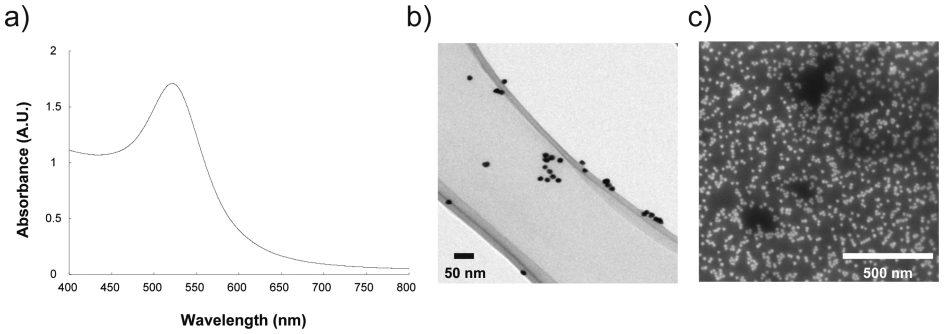

Figure 1. Characterization of the synthesized spherical AuNPs. (a) Surface plasmon absorption of AuNPs with a maximum absorbance at 521.6 nm. (b) TEM image of the synthesized AuNPs and (c) SEM image of the synthesized AuNPs.

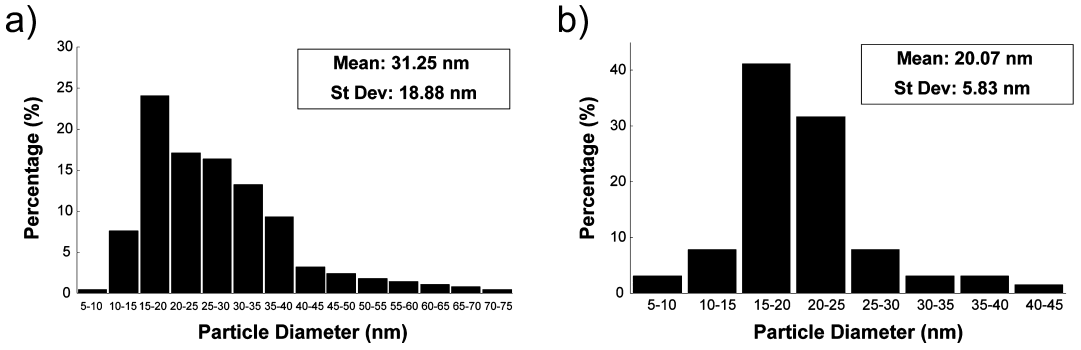

Figure 2. Characterization of synthesized AuNPs. (a) DLS analysis of synthesized AuNPs. (b) Particle size distribution driven from TEM images.

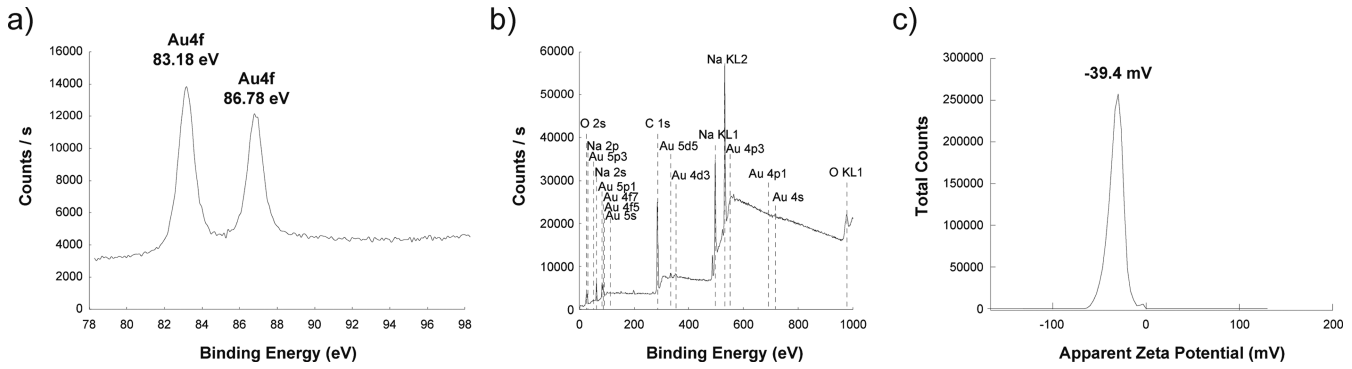

Figure 3. Characterization of synthesized AuNPs. (a,b) XPS spectra. (c) Zeta potential of synthesized AuNPs.

applications to be developed. Although, until now, both theoretical and experimental approaches are used for evaluating and measuring photothermal heat generation from the surface of the AuNPs, there have not been any regression models developed to decipher the factors that affect heat generation, which would lead to the ability of simulating optothermal energy conversion in surfaces of nanostructures. Therefore, in this work, we have experimentally measured the heat generation in AuNPs that have been exposed to continuous LASER illumination and have analyzed the experimental results based on a statistical method to further develop a mathematical model that allows predicting AuNP heat generation and temperature changes in the system. Furthermore, we statistically evaluated the effect of different important factors such as laser power (consequently power intensity), illumination time, AuNP concentration in an aqueous solution, and their interactions. This led to the development of an accurate mathematical equation that predicts the amount of heat generation in a AuNP solution after being exposed to laser light.

2. RESULTS AND DISCUSSION

2.1. AuNPs Characterization. The initial characterization of the AuNPs was done by UV−visible absorption spectroscopy. For metallic NPs, absorption wavelengths in the range of 300−800 nm are normally used for their characterization.[26] However, the UV−vis spectra of the reaction sample were recorded instantly after the synthesis, and the spectra are shown in Figure 1a. As can be seen, the maximum absorbance of the synthesized AuNPs is at 521.6 nm, which corresponds to the results obtained in the literature for AuNPs.[27−29]

Transmission electron microscopy (TEM) and scanning electron microscopy (SEM) were used for the size and morphological analysis of the synthesized AuNPs. As can be seen from Figure 1b,c, the synthesized particles are mostly spherical and homogenous in size.

https://dx.doi.org/10.1021/acsomega.9b02567
ACS Omega 2020, 5, 1377−1383

Furthermore, a dynamic light scattering (DLS) analysis showed that the average mean size of the AuNPs was 31.25 nm (Figure 2a), while the particle size distribution analysis driven from the analysis of NPs present in the TEM images showed that the average size of the AuNPs was around 20.07 nm (Figure 2b).

Results showed that more than 73% of the synthesized AuNPs (Figure 2b) are similar in size (between 15 and 25 nm) and homogenous. This particle size difference between the analysis of NPs from TEM images and DLS average size measurement is related to the broad distribution formed by mixing two particles in the DLS measurement.[30] Furthermore, Zhang et al.[31] have reported that the average size of NPs obtained from DLS is usually larger than the analysis with TEM, and it is attributed to the influence of Brownian motion of the particles in solution.

The surface scan spectra demonstrated the presence of Au and C atoms according to their binding energies. The most prominent signal in the X-ray photoelectron spectroscopy (XPS) spectrum is the Au 4f consisting of two spin−orbit components at 83.18 and 86.78 eV (Figure 3a).[32,33] In the XPS survey spectrum of the sample surface (Figure 3b), in addition to peaks of Au, photoelectron and Auger peaks of C, O, and Na are detected. Carbon and oxygen are from the sample exposure to normal atmosphere, and Na is from the precursor used in the synthesis. The high-resolution spectrum of Au confirms that the NPs are in their elemental state.

Figure 3c shows the zeta potential measurement of the synthesized AuNPs (with concentration of 88 μg/mL) by the citrate method (no buffer was used in this measurement). The results showed that the zeta potential value is −39.4 mV, which demonstrates that the synthesized AuNPs are considered to be strongly anionic which resulted from using citrate as a capping agent. Moreover, the results show that these NPs have high stability in solution.[34]

2.2. Effect of AuNP Concentration, Illumination Time, and Laser Power on Temperature Changes of an Aqueous AuNP Colloid. In order to decipher the effective variables affecting temperature increase in a AuNP aqueous colloid, a Pareto analysis was used, taking into account three factors and their interactions. In this case, a reference line exists in the chart that indicates statistical significance of a factor. Indeed, bars that cross this reference line are considered to be statistically significant.

The Pareto chart in Figure 4 shows that the main effect of all factors was significant at a level of 0.05. In addition to the mentioned effects, the effect of time × laser power was the only significant interaction effect observed.

Next, in order to investigate how the variables affect the response and what was the relationship between the variables and their response, a regression analysis was performed. We applied the significant factor identified from the Pareto interpretations, and the relationships were identified between temperature, as a response or dependent variable, and significant factor, as independent variables. The regression model in terms of the coded factors in the form of a linear equation is described as follows

$$y = 13.83 + 1.667x_1 + 0.917x_2 + 5.917x_3 + x_2x_3 \quad (1)$$

where x_1, x_2, x_3, and y represent the concentration of AuNPs solution, time illumination of laser light, laser power, and temperature change, respectively.

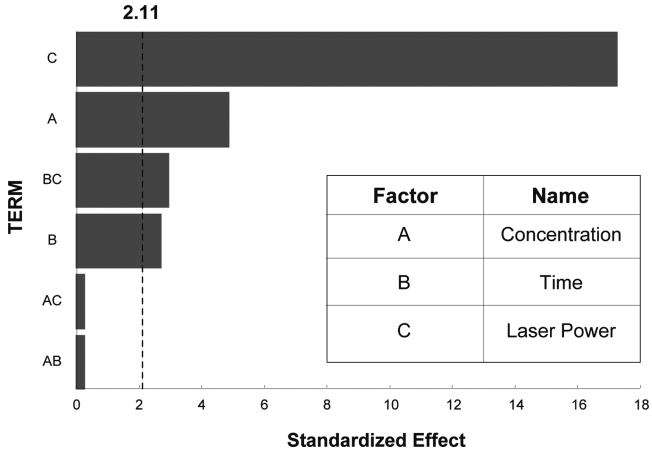

Figure 4. Pareto chart showing the main effects of the various factors and their interaction on the temperature change of the colloidal AuNPs.

ANOVA was also used in the model analysis, and the results can be observed in Table 1. The ANOVA analysis was performed to compare the effect of a significant factor by the parameter variance and an F-test. Statistically, whenever the F value in ANOVA is bigger, the regression coefficient will be bigger in the equation, and consequently, the factor will be more significant and efficacious in response. According to this, it can be observed that the laser power was the most effective factor in a temperature change response in the AuNP colloid because it had the largest coefficient in the model. The effectiveness of laser power in the temperature changes of AuNPs can also be theoretically confirmed from a physics aspect. The theoretical calculations show that the maximum temperature at the surface of a small enough AuNP (where retardation effects can be ignored) is obtained as follows[35]

Table 1. ANOVA Result for the Experimental Parameters Which Affects Temperature of AuNPs Solution[a]

source	DF	adj SS	adj MS	F-Value	P-Value
model	4	951.00	237.750	93.46	0.00000
concentration	1	66.67	66.667	26.21	0.00000
time	1	20.17	20.167	7.93	0.01104
laser power	1	840.17	840.167	330.27	0.00000
time × laser power	1	24.00	24.000	9.43	0.00628
error	19	48.33	2.544		
lack-of-fit	3	11.00	3.667	1.57	0.23523
pure error	16	37.33	2.333		
total	23	999.33			

[a]P-values less than 0.05 indicate model terms are significant.

$$\Delta T_{max}(I_0) = \frac{R_{NP}^2}{3k_0}\mathrm{Re}\left[i\omega\frac{1-\varepsilon(r)}{8\pi}\left|\frac{3_{\varepsilon_0}}{2_{\varepsilon_0}+\varepsilon_m}\right|^2\right]\frac{8\pi\cdot I_0}{C\sqrt{\varepsilon_0}} \quad (2)$$

where R_{NP} and c is the radius of AuNPs and velocity of light, respectively, omega is the frequency of the incident light, K_0 is the thermal conductivity of the solution, $\varepsilon(r)$ is the local dielectric constant, ε_0 is the dielectric constant of the solution, and $\varepsilon(\omega)$ is the frequency-dependent dielectric constant of AuNP. I_0 is the intensity of the LASER beam directly proportional to the LASER power. This equation shows that

https://dx.doi.org/10.1021/acsomega.9b02567
ACS Omega 2020, 5, 1377−1383

Table 2. Predicted and Actual Values of ΔT for the Confirmation the Regression Model

set	laser power (mW)	illumination time (min)	AuNPs concentration (μg/mL)	predicted ΔT (°C)	actual ΔT (°C)[a]	RSE (%)
1	200	20	44	13.1	r_1 = 13 r_2 = 14 r_3 = 14	3.8
2	130	17	60	9.3	r_1 = 9 r_2 = 9 r_3 = 9	1.5
3	250	10	88	17.05	r_1 = 17 r_2 = 17 r_3 = 18	3.2
4	300	20	44	20.01	r_1 = 20 r_2 = 20 r_3 = 22	3.3
5	120	13	50	9.74	r_1 = 10 r_2 = 10 r_3 = 10	2.7

[a] r is replication of experiment.

the temperature of single AuNPs increases linearly with light intensity.

In addition to the laser power, concentration of AuNPs solution was the next most effective variable triggering a temperature change in the bulk solution. The concentration effect can be explained theoretically by considering the physics of ensemble heating. For an ensemble of AuNPs with concentration c, the total volumetric heat flux Q generated by all NPs can be approximated as

$$Q = c \cdot \sigma_{abs} \cdot I_0 \quad (3)$$

where σ_{abs} is the absorption cross-section of single AuNPs. As can be seen, the heat (and so the temperature) is linearly proportional to the concentration. However, LASER light is attenuated in the solution according to the Beer−Lambert law. The characteristic time of NP cooling for the size of our structures is of the order of picosecond to nanosecond.[36] Furthermore time inversely depends on the surrounding medium heat diffusion constant. High diffusion of the surrounding medium (here water) makes this time very short. Consequently, the temperature increase over the solution along the LASER path would be uniform when it comes to time intervals in the order of minutes. The LASER intensity in the solution is exponentially decreased with a decay constant of $\tau = c \cdot \sigma_{abs}$. Considering these two facts indicates that although increasing AuNPs concentration results in a linear increase of the total heat, the intensity is attenuated along with the solution with a higher number of AuNPs.[37]

Finally, the other factors including time × laser-power interaction and time illumination were the next most effective variables in triggering a temperature change response, therefore exhibiting the next biggest coefficient value in the equation.

It should be noted that the positive sign of all significant regression coefficients implied that all the terms had a direct relationship with AuNP temperature change. It indicated that the mean of the dependent factor tended to increase or decrease when the value of each independent variable increased or decreased, consequently. Therefore, more temperature changes and more intensity in the photothermal phenomenon of the AuNPs solution were due to increasing values of each independent variable.

Likewise, the ANOVA regression results showed a statistical significance of the applied model and the lack of fit was investigated by an F-test. Together, these results depicted that the obtained linear model was highly significant (p-value < 0.0001) and a lack of fit showed no significance (p-value > 0.05).

Furthermore, both the correlation coefficient value (95.16%) and adjusted R^2 (94.15%), which indicate the correlation between the model and experimental data, had a large enough value. In other words, they were close to a value of 100% which corresponds to a highly acceptable fit to a linear model from experimental data.

In order to validate the obtained regression model, predicted values of ΔT were obtained based on an uncoded regression model (Table 2). Then, the average of experimental data was compared to predicted values by calculating the RSE % (eq 4). The results of RSE % showed that the difference between experimental and predicted values were no significant (RSE values were lower than 4). However, there was a very good fit between the linear model and the experimental data. Hence, the model can be used to determine ΔT with good accuracy and precision in the range of the values of the factors.

It should be highlighted that when water, as a negative control, was exposed to the laser light, there was not a distinguishable change in temperature. This means that all of the increased temperatures shown in the AuNPs colloids were triggered by the optical properties of the AuNPs.

3. CONCLUSIONS

In this paper, we designed an experiment based on a plasmonic photothermal heating feature observed in AuNPs. These optical properties allow the AuNPs to heat up their surroundings and have applications in diverse systems, including biomaterial production and gene silencing.

In this manuscript, after the synthesis and characterization of AuNPs, we experimentally measured the heat generation of AuNPs under CW LASER illumination and made a temperature profile. Based on a statistical evaluation, we identified different crucial factors that are effective in temperature change of AuNPs solution. Our results indicated that the laser power, concentration of AuNPs, time × laser power interaction, and time illumination, were the most effective in achieving temperature changes of AuNPs colloids. Further, we applied the significant variables to present a regression model in order to predict the heat generation amount from the same AuNPs

https://dx.doi.org/10.1021/acsomega.9b02567
ACS Omega 2020, 5, 1377−1383

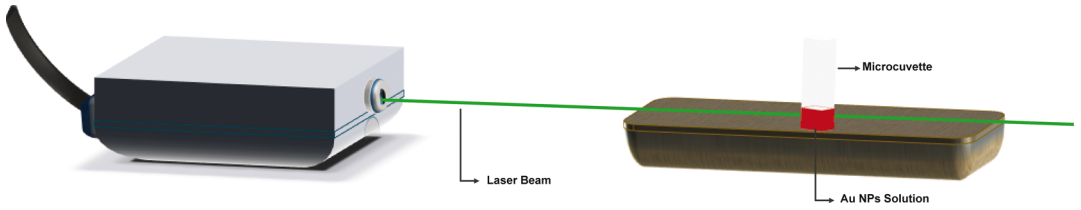

Figure 5. Experimental setup for measuring the temperature profile of AuNP solutions.

surface. This model was chosen according to the *F* test, lack-of-fit-test, and was adjusted with the R^2 value. The RSE % values observed from our model were lower than 4%, demonstrating that the model accurately describes ΔT of AuNP colloids within the range of the values of the factors. In addition, these results were confirmed and justified theoretically. The results and model reported in this work will aid research in the development of systems that incorporate localized heating through the exposure of specific wavelengths.

4. MATERIALS AND METHODS

4.1. Materials. Gold trichloride ≥99.99% trace metals basis ($AuCl_3$) and trisodium citrate dihydrate ($Na_3C_6H_5O_7{\cdot}2H_2O$) were purchased from Merck. Deionized water was used in all experiments. A UV−vis spectrophotometer (LMAI-1-ES-3) from Thermo Spectronic, professional multimeter RMS, and a continue wave green laser (Quantum, model excel+mpc6000) with a peak wavelength of 532 nm and beam size of 1.48 mm were used.

4.2. Synthesis of AuNPs. To synthesize AuNPs, the Turkevich et al.[38] method using a citrate reduction was used.[39] Aqueous gold chloride solution (0.5 mM) (300 mL) was prepared in a beaker and was boiled on heated stirred plate until boil. As soon as boiling was observed, 30 mL of an aqueous 38.8 mM trisodium citrate solution was added to the beaker and immediately after adding the trisodium citrate solution, the colorless solution first turned dark violet-red followed by a maroon color. Finally, the synthesized AuNP solution was brought to room temperature to cool down, and the maroon color solution slowly turned ruby red in color.

4.3. Characterization of the Obtained AuNPs. Among the different techniques to characterize NPs, UV−vis spectroscopy,[31] zeta potential analysis, and transmission electron microscope are the most common. The UV−vis spectroscopy technique is a very useful, applicable, and reliable method for the primary characterization of synthesized AuNPs. Therefore, the optical absorption spectra of colloidal AuNPs were measured using this technique. TEM and SEM were also used for the characterization of the AuNPs to determine their shape and morphology. DLS was used to determine the size of the synthesized gold particles and estimate the particle size distribution profile.

XPS was carried out to investigate the elemental composition and chemical states of the synthesized NPs. We used a Thermo Scientific K-Alpha XPS instrument. Finally, we used a Zetasizer (Nano ZS90 model) to determine stability of the AuNPs in solution.

4.4. Setup of the Laser to Determine the Temperature Profile Measurements. To obtain a complete temperature profile, a CW green laser (532 nm wavelength) was employed to expose an aqueous homogeneous dispersion of AuNPs (Figure 5). Suspensions (200 μL) of AuNPs were loaded in a semimicro UV-cuvette (cat. no. 7591 50) and were directly illuminated with the CW green laser. Moreover, deionized water as a control experiment in the same volume (200 μL) was loaded in the same cuvette and was also illuminated by the CW green laser (532 nm wavelength). The temperature was measured before and after laser illumination using a professional RMS Digital Multimeter sensitive sensor, and then, the temperature changes between the initial and final illumination time were recorded.

4.5. Statistical Analysis. The experimental design was carried out using the MINITAB statistical software version 18, and it was based on a full factorial design. Factorial designs are preferred over the traditional one factor designs when involving a time method because they offer better estimates on the effect of each factor, and it allows the easy estimate of the interactive effect between the factors, therefore offering more experimental information using fewer resources (i.e., time, material).

In this study, the design included three separate factors at several levels, and they were performed in triplicates. The factors included the CW laser with two different powers (100 and 300 mW), two AuNP aqueous concentrations (the AuNP concentration were calculated by stoichiometries calculations and checked with an online NP conversion calculator (www.nanocomposix.com)) at 44 and 88 μg/mL; and finally another factor tested at two levels was the exposure time (10 and 20 min).

In order to identify the effective variables that induced a temperature change in the AuNPs solution, the Pareto analysis was used. In order to illustrate how these factors affect the temperature change registered in the AuNPs solution, a regression model was developed, and the related analysis was done. All of the experiments were analyzed at a 95% confidence interval using the MINITAB statistical software.

In addition, in order to investigate the regression model performance, five random tests were performed in three replicates and the residual standard error percentage (RSE %) was calculated (eq 4) as follows[40]

$$\text{Residual standard error}(\%) = \frac{(\text{actual value} - \text{predicted value})}{\text{predicted value}} \times 100 \quad (4)$$

AUTHOR INFORMATION

Corresponding Authors

Abbas Alemzadeh − *Shiraz University, Shiraz, Iran*; Phone: +98 713 2286134; Email: alemzadeh@shirazu.ac.ir

José Rubén Morones Ramírez − *Universidad Autónoma de Nuevo León, UANL. Facultad de Ciencias Químicas, San Nicolás de los Garza, Mexico, and Centro de Investigación en Biotecnología y Nanotecnología, Facultad*

https://dx.doi.org/10.1021/acsomega.9b02567
ACS Omega 2020, 5, 1377−1383

de Ciencias Químicas, Universidad Autónoma de Nuevo León, Apodaca, Mexico; orcid.org/0000-0001-7009-686X; Phone: +52-818-329-4000 ext. 3439; Email: jose.moronesrmr@uanl.edu.mx

Other Authors

Nahid Rafiei − *Universidad Autónoma de Nuevo León, UANL. Facultad de Ciencias Quimicas, San Nicolás de los Garza, Mexico, Centro de Investigación en Biotecnologia y Nanotecnologia, Facultad de Ciencias Químicas, Universidad Autónoma de Nuevo León, Apodaca, Mexico, and Shiraz University, Shiraz, Iran*

Hossein Alishah Aratboni − *Universidad Autónoma de Nuevo León, UANL. Facultad de Ciencias Químicas, San Nicolás de los Garza, Mexico, and Centro de Investigación en Biotecnologia y Nanotecnologia, Facultad de Ciencias Químicas, Universidad Autónoma de Nuevo León, Apodaca, Mexico*

Larousse Khosravi Khorashad − *University of California, San Diego, La Jolla, California;* orcid.org/0000-0003-0461-5638

Sadasivan Shaji − *Universidad Autónoma de Nuevo León, UANL. Facultad de Ingenieria Mecánica y Eléctrica, San Nicolás de los Garza, Mexico;* orcid.org/0000-0001-7745-0796

Complete contact information is available at: https://pubs.acs.org/10.1021/acsomega.9b02567

Author Contributions

¶N.R. and H.A.A. contributed equally to the work.

Notes

The authors declare no competing financial interest.

■ ACKNOWLEDGMENTS

This work was supported by financial support through Paicyt 2019-2020, a Science Grant from the Universidad Autónoma de Nuevo León, and CONACyT Grants for Basic science grant 221332, Fronteras de la Ciencia grant 1502, and Infraestructura grant 279957.

■ REFERENCES

(1) Nikalje, A. P. Nanotechnology and its applications in medicine. *Med. Chem.* **2015**, *5*, 081−089.
(2) Maher, K. O. Nanomedicine and nanotechnology for heart failure research, diagnosis, and treatment. *Heart Failure in the Child and Young Adult*; Elsevier, 2018; pp 779−784.
(3) Dursun, S.; Kaya, I. C.; Kalem, V.; Akyildiz, H. UV/visible light active CuCrO 2 nanoparticle−SnO 2 nanofiber p−n heterostructured photocatalysts for photocatalytic applications. *Dalton Trans.* **2018**, *47*, 14662−14678.
(4) Ji, X.; Wang, J.; Mei, L.; Tao, W.; Barrett, A.; Su, Z.; Wang, S.; Ma, G.; Shi, J.; Zhang, S. Porphyrin/SiO2/Cp* Rh (bpy) Cl Hybrid nanoparticles mimicking chloroplast with enhanced electronic energy transfer for biocatalyzed artificial photosynthesis. *Adv. Funct. Mater.* **2018**, *28*, 1705083.
(5) Nasrollahzadeh, M.; Issaabadi, Z.; Tohidi, M. M.; Mohammad Sajadi, S. Recent progress in application of graphene supported metal nanoparticles in C− C and C− X coupling reactions. *Chem. Rec.* **2018**, *18*, 165−229.
(6) Kwak, S.-Y.; Lew, T. T. S.; Sweeney, C. J.; Koman, V. B.; Wong, M. H.; Bohmert-Tatarev, K.; Snell, K. D.; Seo, J. S.; Chua, N.-H.; Strano, M. S. Chloroplast-selective gene delivery and expression in planta using chitosan-complexed single-walled carbon nanotube carriers. *Nat. Nanotechnol.* **2019**, *14*, 447.
(7) Gaul, R.; Ramsey, J. M.; Heise, A.; Cryan, S.-A.; Greene, C. M. Nanotechnology approaches to pulmonary drug delivery: Targeted delivery of small molecule and gene-based therapeutics to the lung. *Design of Nanostructures for Versatile Therapeutic Applications*; Elsevier, 2018; pp 221−253.
(8) Cunningham, F. J.; Goh, N. S.; Demirer, G. S.; Matos, J. L.; Landry, M. P. Nanoparticle-mediated delivery towards advancing plant genetic engineering. *Trends Biotechnol.* **2018**, *36*, 882−897.
(9) Alishah, H.; Pourseyedi, S.; Ebrahimipour, S. Y.; Mahani, S. E.; Rafiei, N. Green synthesis of starch-mediated CuO nanoparticles: preparation, characterization, antimicrobial activities and in vitro MTT assay against MCF-7 cell line. *Rendiconti Lincei. Mat. Appl.* **2017**, *28*, 65−71.
(10) Alishah, H.; Pourseyedi, S.; Mahani, S. E.; Ebrahimipour, S. Y. Extract-mediated synthesis of Ag@ AgCl nanoparticles using Conium maculatum seeds: characterization, antibacterial activity and cytotoxicity effect against MCF-7 cell line. *RSC Adv.* **2016**, *6*, 73197−73202.
(11) Alishah, H.; Seyedi, S. P.; Ebrahimipour, S. Y.; Esmaeili-Mahani, S. A green approach for the synthesis of silver nanoparticles using root extract of Chelidonium majus: characterization and antibacterial evaluation. *J. Cluster Sci.* **2016**, *27*, 421−429.
(12) Chugh, H.; Sood, D.; Chandra, I.; Tomar, V.; Dhawan, G.; Chandra, R. Role of gold and silver nanoparticles in cancer nano-medicine. *Artif. Cells, Nanomed., Biotechnol.* **2018**, *46*, 1210−1220.
(13) Peng, J.; Liang, X. Progress in research on gold nanoparticles in cancer management. *Medicine* **2019**, *98*, No. e15311.
(14) Martinkova, P.; Brtnicky, M.; Kynicky, J.; Pohanka, M. Iron oxide nanoparticles: innovative tool in cancer diagnosis and therapy. *Adv. Healthcare Mater.* **2018**, *7*, 1700932.
(15) He, M.; Yan, Y.; Pei, F.; Wu, M.; Gebreluel, T.; Zou, S.; Wang, C. Improvement on lipid production by Scenedesmus obliquus triggered by low dose exposure to nanoparticles. *Sci. Rep.* **2017**, *7*, 15526.
(16) Roper, D. K.; Ahn, W.; Hoepfner, M. Microscale heat transfer transduced by surface plasmon resonant gold nanoparticles. *J. Phys. Chem. C* **2007**, *111*, 3636−3641.
(17) Rashidi-Huyeh, M.; Palpant, B. Thermal response of nanocomposite materials under pulsed laser excitation. *Jpn. J. Appl. Phys.* **2004**, *96*, 4475−4482.
(18) Hechler, D.; Nitsch, R.; Hendrix, S. Green-fluorescent-protein-expressing mice as models for the study of axonal growth and regeneration in vitro. *Brain Res. Rev.* **2006**, *52*, 160−169.
(19) Jung, I.; Kim, M.; Kwak, M.; Kim, G.; Jang, M.; Kim, S. M.; Park, D. J.; Park, S. Surface plasmon resonance extension through two-block metal-conducting polymer nanorods. *Nat. Commun.* **2018**, *9*, 1010.
(20) Fan, W.; Leung, M. Recent development of plasmonic resonance-based photocatalysis and photovoltaics for solar utilization. *Molecules* **2016**, *21*, 180.
(21) Garcia, V. B.; de Carvalho, T. G.; da Silva Gasparotto, L. H.; da Silva, H. F. O.; de Araújo, A. A.; Guerra, G. C. B.; Schomann, T.; Cruz, L. J.; Chan, A. B.; de Araújo Júnior, R. F. Environmentally compatible bioconjugated gold nanoparticles as efficient contrast agents for inflammation-induced cancer imaging. *Nanoscale Res. Lett.* **2019**, *14*, 166.
(22) Becker, A.; Leskau, M.; Schlingmann-Molina, B. L.; Hohmeier, S. C.; Alnajjar, S.; Escobar, H. M.; Ngezahayo, A. Publisher Correction: Functionalization of gold-nanoparticles by the Clostridium perfringens enterotoxin C-terminus for tumor cell ablation using the gold nanoparticle-mediated laser perforation technique. *Sci. Rep.* **2019**, *9*, 4150.
(23) Ashley, M. J.; Bourgeois, M. R.; Murthy, R. R.; Laramy, C. R.; Ross, M. B.; Naik, R. R.; Schatz, G. C.; Mirkin, C. A. Shape and size control of substrate-grown gold nanoparticles for surface-enhanced raman spectroscopy detection of chemical analytes. *J. Phys. Chem. C* **2018**, *122*, 2307−2314.

(24) Huang, X.; El-Sayed, M. A. Gold nanoparticles: optical properties and implementations in cancer diagnosis and photothermal therapy. *J. Adv. Res.* **2010**, *1*, 13−28.
(25) Lee, S. E.; Liu, G. L.; Kim, F.; Lee, L. P. Remote optical switch for localized and selective control of gene interference. *Nano Lett.* **2009**, *9*, 562−570.
(26) Mulvaney, P. Surface plasmon spectroscopy of nanosized metal particles. *Langmuir* **1996**, *12*, 788−800.
(27) Zuber, A.; Purdey, M.; Schartner, E.; Forbes, C.; van der Hoek, B.; Giles, D.; Abell, A.; Monro, T.; Ebendorff-Heidepriem, H. Detection of gold nanoparticles with different sizes using absorption and fluorescence based method. *Sens. Actuators, B* **2016**, *227*, 117−127.
(28) Alba-Molina, D.; Martín-Romero, M.; Camacho, L.; Giner-Casares, J. Ion-Mediated Aggregation of Gold Nanoparticles for Light-Induced Heating. *Appl. Sci.* **2017**, *7*, 916.
(29) Dasari, T. S.; Zhang, Y.; Yu, H. Antibacterial activity and cytotoxicity of gold (I) and (III) ions and gold nanoparticles. *Biochem. Pharmacol.* **2015**, *4*, 199.
(30) Souza, T. G. F.; Ciminelli, V. S. T.; Mohallem, N. D. S. A comparison of TEM and DLS methods to characterize size distribution of ceramic nanoparticles. *J. Phys: Conference Series* **2016**, *733*, 012039.
(31) Zhang, X.-F.; Liu, Z.-G.; Shen, W.; Gurunathan, S. Silver nanoparticles: synthesis, characterization, properties, applications, and therapeutic approaches. *Int. J. Mol. Sci.* **2016**, *17*, 1534.
(32) Abdulla-Al-Mamun, M.; Kusumoto, Y.; Mihata, A.; Islam, M. S.; Ahmmad, B. Plasmon-induced photothermal cell-killing effect of gold colloidal nanoparticles on epithelial carcinoma cells. *Photochem. Photobiol. Sci.* **2009**, *8*, 1125−1129.
(33) Ghodake, G. S.; Deshpande, N. G.; Lee, Y. P.; Jin, E. S. Pear fruit extract-assisted room-temperature biosynthesis of gold nanoplates. *Colloids Surf., B* **2010**, *75*, 584−589.
(34) Pongsuchart, M.; Danladkaew, C.; Khomvarn, T.; Sereemaspun, A. *Effect of Glutathione-Stabilized Gold Nanoparticles in 3T3 Fibroblast Cell*; International Conference on Clean and Green Energy IPCBEE, 2012.
(35) Govorov, A. O.; Zhang, W.; Skeini, T.; Richardson, H.; Lee, J.; Kotov, N. A. Gold nanoparticle ensembles as heaters and actuators: melting and collective plasmon resonances. *Nanoscale Res. Lett.* **2006**, *1*, 84.
(36) Metwally, K.; Mensah, S.; Baffou, G. Fluence threshold for photothermal bubble generation using plasmonic nanoparticles. *J. Phys. Chem. C* **2015**, *119*, 28586−28596.
(37) Naccache, R.; Mazhorova, A.; Clerici, M.; Piccoli, R.; Khorashad, L. K.; Govorov, A. O.; Razzari, L.; Vetrone, F.; Morandotti, R. Terahertz thermometry: Combining hyperspectral imaging and temperature mapping at terahertz frequencies. *Laser Photonics Rev.* **2017**, *11*, 1600342.
(38) Turkevich, J.; Stevenson, P. C.; Hillier, J. A study of the nucleation and growth processes in the synthesis of colloidal gold. *Discuss. Faraday Soc.* **1951**, *11*, 55−75.
(39) Khlebtsov, B. N.; Khlebtsov, N. G. On the measurement of gold nanoparticle sizes by the dynamic light scattering method. *Colloid J.* **2011**, *73*, 118−127.
(40) Farooqui, M.; Hassali, M. A.; Shatar, A. K. A.; Farooqui, M. A.; Saleem, F.; Haq, N. u.; Othman, C. N. Use of complementary and alternative medicines among Malaysian cancer patients: A descriptive study. *J. Tradit., Complementary Med.* **2016**, *6*, 321−326.

https://dx.doi.org/10.1021/acsomega.9b02567
ACS Omega 2020, 5, 1377−1383